ELSEVIER

Journal of Nuclear Materials 264 (1999) 216–227

journal of nuclear materials

Alloying effects on the corrosion behavior of binary Nb-based and Mo-based alloys in liquid Li

Jun-ichi Saito [a,*], Satoshi Inoue [b], Shigeki Kano [a], Toshikatsu Yuzawa [c], Mitsuaki Furui [d], Masahiko Morinaga [d]

[a] *Oarai Engineering Center, Power Reactor and Nuclear Fuel Development Corporation, 4002 Narita, Oarai-machi, Higashi-Ibaraki-gun, Ibaraki 311-1393, Japan*

[b] *Department of Mechanical Engineering, Numazu College of Technology, 3600 Ooka, Numazu 410-0022, Japan*

[c] *Department of Production Systems Engineering, Toyohashi University of Technology, Toyohashi, Aichi 441-8580, Japan*

[d] *Department of Materials Science and Engineering, School of Engineering, Nagoya University, Furo-cho Chikusa-ku, Nagoya 464-8603, Japan*

Received 29 March 1996; accepted 11 June 1998

Abstract

Alloying effects on the corrosion in liquid Li at 1473 K have been investigated for both binary Nb-based and Mo-based alloys. For the binary Nb-based alloys, the weight change due to the corrosion varied largely with alloying elements. Also, there was a clear difference in the surface morphology between them after corrosion tests. Either one or two corrosion products and large cracks were observed on the surface of all the Nb-based alloys. The weight change of a Nb–Hf alloy was the smallest among a variety of Nb-based alloys, indicating that the Hf addition was very effective in improving the corrosion resistance. On the other hand, for the binary Mo-based alloys the weight change was about a factor of 10 smaller than that for the binary Nb-based alloys. There were no cracks and a little corrosion products on the surface of them, indicating that the Mo-based alloys have much superior corrosion resistance in liquid Li than the Nb-based alloys.

PACS: 28.41.Qb; 81.65.Kn

1. Introduction

Both the Nb-based and the Mo-based alloys are promising materials for structural applications in advanced nuclear plants. In particular, they are expected to be one of the super-heat resisting materials durable even in severe nuclear environments of fast breeder reactor. They are required to have an excellent combination of high temperature strength and good corrosion resistance against liquid alkali metals. The effects of interstitial impurities on the mechanical properties have been reported for Nb-based alloys [1,2]. Also, it is known that the oxygen impurity affects significantly the corrosion resistance of Nb-based alloys [3]. Recently, corrosion behavior in liquid Li has been investigated of Nb–1 wt% Zr and PWC-11 (Nb–1 wt% Zr–0.1 wt% C) [4]. However, there has not been any study of alloying effects on the corrosion resistance of Nb-based and Mo-based alloys. Also, for alloy design it is really necessary to get basic information of the corrosion in liquid metals at high temperature. In our previous study, alloying effects on the corrosion resistance against liquid Na at 923 K were examined in Nb-based alloys [5]. In the present study, alloying effects on the corrosion behavior of both the Nb-based and the Mo-based alloys were first investigated using a capsule test in liquid Li. A series of corrosion tests was carried out in liquid Li at 1473 K, and beneficial elements for improving corrosion resistance were proposed on the basis of these experimental results.

* Corresponding author. E-mail: saito@oec.pnc.go.jp.

0022-3115/99/$ – see front matter
PII: S0022-3115(98)00460-7

2. Experimental procedure

2.1. Specimens and corrosion test

The binary Nb-based and the Mo-based alloys used in the present experiments were Nb–5 at.% M (M: Mo, Ru, Hf, Ta, W, Re), and Mo–5 at.% M (M: Nb, Ru, Hf, Ta, W, Re). All these alloying elements, M, have a large solid solubility Nb or Mo, and their addition can improve the mechanical strength and the weldability of pure metals. A commercial alloy, Nb–1 wt% Zr, was also used as a reference alloy in this study. These alloys were melted using a tri-arc furnace in a high purity Ar gas atmosphere. Every raw material had a purity higher than 99.9%. After arc-melting, homogenized heat treatment was carried out at 1773 K for 3.6 ks in vacuum. The specimens for corrosion tests were then cut into the size of 10 mm square and 2 mm thick. The specimen surface was polished using a #1200 emery paper.

The corrosion tests were performed by setting the specimen in the capsule which was filled with liquid Li and heating it at 1473 K for 1.08 Ms. Fig. 1 shows the appearance of the inner capsule and the specimen holder used for the present corrosion tests. Employing this equipment, 12 specimens were able to be tested at the same time. The inner capsule was set inside the outer capsule. This system of double capsules, which are made of Nb–1 wt% Zr, guarantees against the leakage of liquid Li to the outside. Every operation for setting-up and taking-out of specimens was performed in the high purity Ar gas atmosphere in a glove-box. The gas concentration of O_2, N_2 and H_2O in the glove-box were controlled so that the oxygen concentration <1 ppm, the nitrogen concentration <100 ppm, and the moisture concentration <25 ppm. During the corrosion test at 1473 K, the capsule system was held in a high purity Ar gas atmosphere. The chemical compositions of liquid Li measured before corrosion tests were shown in Table 1. Two kinds of liquid Li were used in this experiment.

2.2. Micro-analysis before and after corrosion tests

The specimen size was measured accurately using a micrometer before corrosion tests. The weight of the specimen was also measured using a high-precision balance before and after corrosion tests. The accuracy of the weight measurement was better than 13×10^{-6} g. The surface morphology of the specimen was observed using optical microscope at the interval of every 0.36 Ms during the corrosion test. After 1.08 Ms, the surface morphology, the microstructure and the composition of corrosion products were examined by scanning electron microscopy (SEM), electron probe micro-analysis (EPMA) and X-ray diffraction methods.

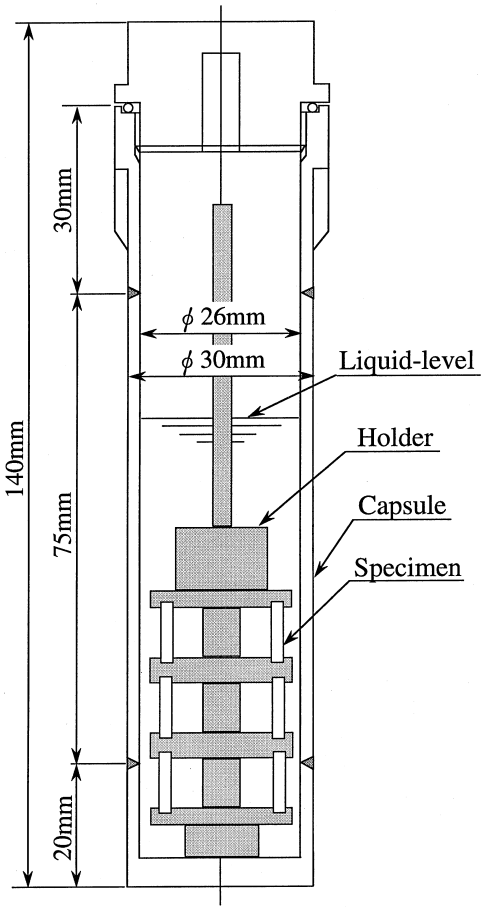

Fig. 1. Capsule and specimen-holder used for corrosion test.

3. Results

3.1. Weight changes due to the corrosion in liquid Li

The weight changes with the corrosion time are shown in Fig. 2 for the Nb-based binary alloys. Here, a plus sign of the weight change means the weight gain, whereas a minus sign means the weight loss. The two results of a reference alloy, Nb–1Zr, are shown in this figure in order to check the reproducibility of the experimental data. From this figure, it was apparent that Nb–Mo and Nb–W alloys showed the weight gain, but

Table 1
Results of the chemical analysis of impurities in Li before corrosion test (wt ppm)

Lot No.	Elements					
	Ca	Fe	Mg	K	Na	N
1	20	20	10	10	80	90
2	40	10	10	10	40	30

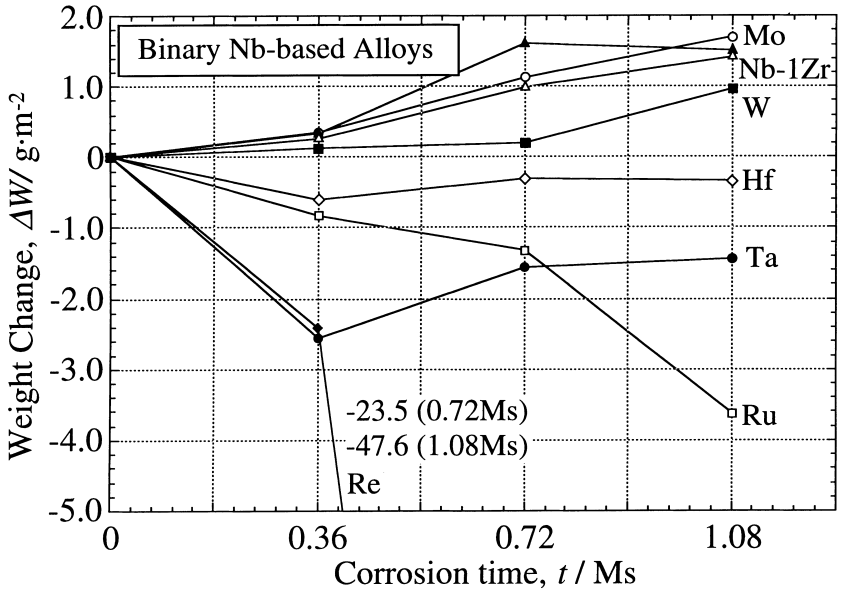

Fig. 2. Weight change of Nb-based alloys with corrosion time.

Nb–Hf, Nb–Ta, Nb–Ru and Nb–Re alloys showed the weight loss. In particular, Nb–Re alloy showed the largest weight loss among them, and sometimes it was broken into small chips in the edge of the specimen due to very severe corrosion. In contrast to this, the Nb–Hf alloy showed a moderate weight change. Nb–1Zr alloy showed the weight gain, which was comparable to that of the Nb–Mo alloy.

The result for the Mo-based binary alloys are shown in Fig. 3 together with the results of a reference alloy, Nb–1Zr, which was tested with the Mo-based alloys in the same capsule. All the Mo alloys showed the weight gain except for a Mo–Ru alloy. The weight change of the Mo–Hf alloy was very small, similar to the result of the Nb–Hf alloy. The Nb–1Zr alloys showed the much larger weight gain, as compared to the Mo–based alloys.

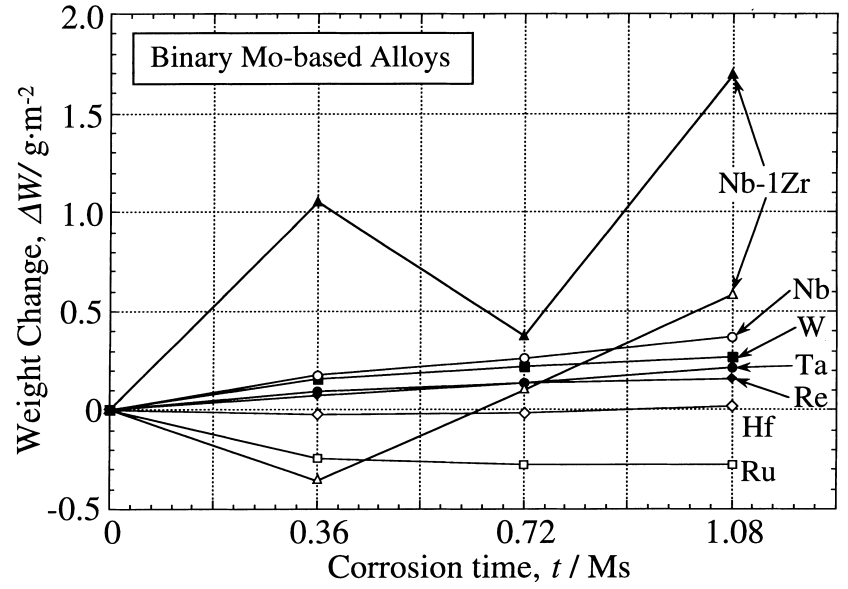

Fig. 3. Weight change of Mo-based alloys with corrosion time.

The corrosion curve of the Nb–1Zr alloy shown in Fig. 3 was different in some way from the result shown in Fig. 2, probably due to the difference in the alloy specimens tested together in the capsule. However, still the weight change after 1.08 Ms lay at the similar level between them.

There was a strong dependence of the weight change on the alloying elements in both alloy systems. Also, the Mo-based alloys exhibited about 10 times smaller weight change than the Nb-based alloys. Thus, the corrosion resistance against liquid Li was more excellent for the Mo-based alloys than for the Nb-based alloys. In addition, there were a few resemblances in the corrosion behavior between these two alloy systems. For example, Hf-containing alloys exhibited the smallest weight change, and Ru-containing alloys showed the weight loss in both alloy systems.

3.2. Evolution of surface morphology with corrosion time

The surface morphology was observed using optical microscopy at every 0.36 Ms in the corrosion process. The morphological evolution of the specimen surface with corrosion time was traced, while keeping attention to the same small region throughout the observation. The initial surface morphology prior to the corrosion test is shown in Fig. 4 for Nb–1Zr alloy. All the specimen had similar initial surface morphology.

3.2.1. Nb-based alloys

The appearances of the surfaces of the Nb-based alloys are shown in Fig. 5. Three micrographs in each column showed the respective surface morphology after the corrosion tests for 0.36, 0.72 and 1.08 Ms. The traces of polishing flaws shown in Fig. 4 were no longer observed in these micrographs. However, for example, as shown in (a), straight cracks ran through the surface of the Nb–Mo alloy even after the short term test for 0.36 Ms, and they appeared independent of grain boundaries. Also, they became wider, and their number on the surface increased with increasing corrosion time. A corrosion product indicated by A in the bottom micrograph of (a) grew up on the surface and the number increased significantly after the test for 1.08 Ms. The surface morphology of Nb–Ta and Nb–W alloys was nearly similar to that of Nb–Mo alloy. However, the corrosion product grew more quickly in these alloys than in the Nb–Mo alloy.

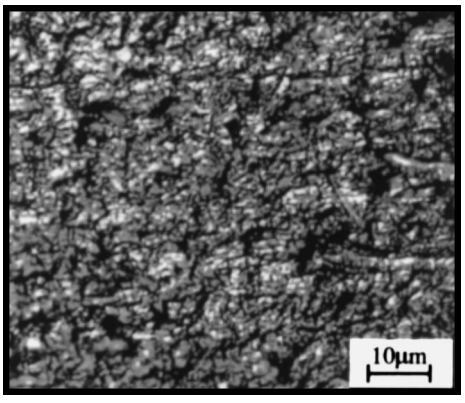

Fig. 4. Surface morphology of Nb–1Zr alloy observed prior to corrosion test.

There were many and large corrosion products on the surface of the Nb–Ru alloy after the test for 0.36 Ms as was indicated by A in Fig. 5(a). The curved cracks also ran through the surface, independent of grain boundaries and they sometimes cut through the corrosion products. As the corrosion proceeded, the corrosion products grew up and the cracks were further widened. After 0.72 Ms, formed were some fine corrosion products as indicated by B in the micrograph. Thus, two types of the corrosion products coexisted on the surface of this alloy. The Nb–Re alloy was similar in the surface morphology to the Nb–Ru alloy.

The surface morphology of the Nb–Hf alloy was shown in Fig. 5(c). The large gains were observed in this alloy. The appearance of the surface did not change with the corrosion time, and no corrosion product was seen on the surface. Only the intergranular corrosion took place slightly in it. Also, the cracks were observed in some parts of the specimen, although they were scarcely seen in these micrographs.

The uniform corrosion took place in the Nb–1Zr alloy as shown in Fig. 5(d). The grain boundaries in the A and the B regions shown in the micrographs moved with the corrosion time at 1473 K. This phenomenon will be interpreted as due to the grain growth. There were a little corrosion products on the surface after the test for 1.08 Ms. Also, cracks were observed as shown in the bottom micrograph of (d). This surface morphology was approximately similar to that of the Nb–Hf alloy.

3.2.2. Mo-based alloys

The surface morphology of the Mo–Nb alloy is shown in Fig. 6(a). The fine corrosion products indicated by A in the micrograph were observed on the surface of the specimen after the corrosion test for 0.36 Ms. The size and the number of these products increased with the corrosion time. However, there were no cracks on the surface, which was clearly different from the result of the Nb-based alloys. A similar surface morphology was also observed in Mo–W, Mo–Re and Mo–Ta alloys.

As shown in Fig. 6(b) large corrosion products were formed along the grain boundary and also inside the grain of the Mo–Ru alloy. The size and the number of these products increased with increasing corrosion time.

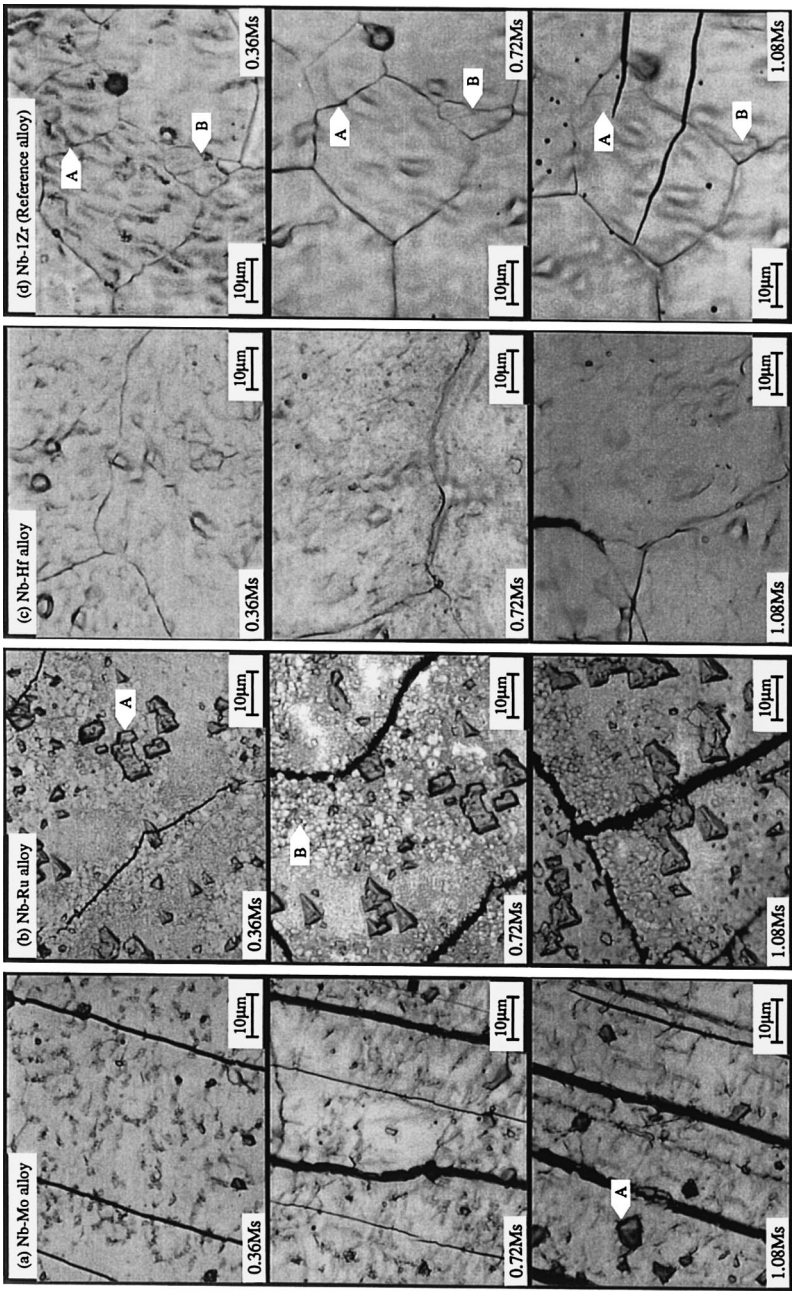

Fig. 5. Evolution of surface morphology for Nb-based alloys with corrosion time: (a) Nb–Mo; (b) Nb–Ru; (c) Nb–Hf; and (d) Nb–1Zr alloys. For each column, top, middle and bottom micrographs were taken in the course of corrosion time for 0.36, 0.72 and 1.08 Ms, respectively.

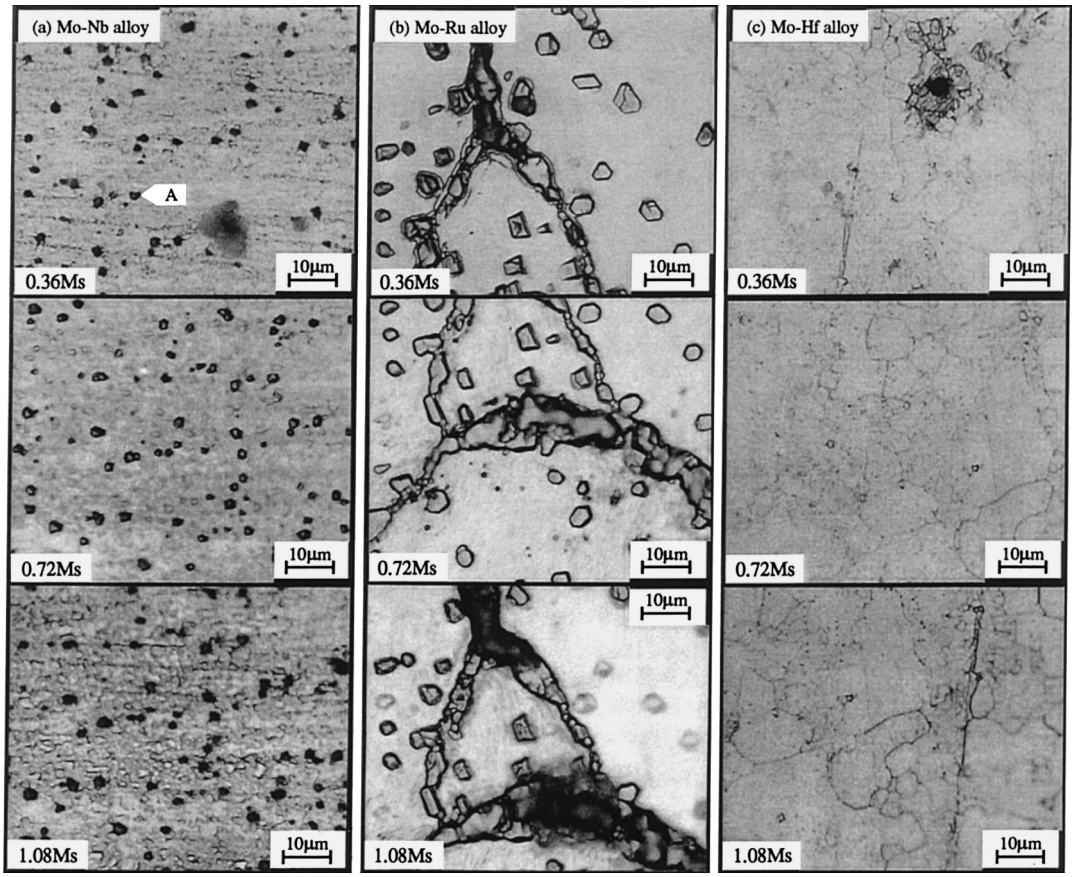

Fig. 6. Evolution of surface morphology for Mo-based alloys with corrosion time: (a) Mo–Nb; (b) Mo–Ru; and (c) Mo–Hf alloys. For each column, top, middle and bottom micrographs were taken in the course of corrosion time for 0.36, 0.72 and 1.08 Ms, respectively.

Also, corrosion products were scarcely observed on the surface of the Mo–Hf alloy as shown in Fig. 6(c). There was a very small change in the surface morphology with corrosion time, even though grain boundaries were etched slightly after the test for 1.08 Ms.

It is noted here that the surface morphology changed part to part in the Mo-based alloys. Four micrographs taken in some regions are shown in Fig. 7. For example, the corrosion product of the Mo–Nb alloy, indicated by A in Fig. 6(a), was nearly absent in the region shown in Fig. 7(a). This was also the case of the Mo–Re alloy as shown in Fig. 7(d). The grain boundary corrosion products scarcely existed in the region of the Mo–Ru alloy are shown in Fig. 7(b), which was a great contrast to the observation shown in Fig. 6(b). In addition, a small amount of the corrosion product was seen in the region of the Mo–Hf alloy shown in Fig. 7(c), which was slightly different from the observation shown in Fig. 6(c). Thus, compared to the corrosion of the Nb-based alloys, more non-uniform corrosion may be characteristic of the Mo-based alloys.

3.3. X-ray diffraction patterns

3.3.1. Nb-based alloys

The X-ray diffraction patterns is shown in Fig. 8(a) for the Nb–Mo alloy. There were a few peaks in addition to the strong peaks of bcc Nb. They were identified with the peaks originated from ZrN. Such extra peaks also appeared in the X-ray diffraction patterns of Nb–Ta and Nb–W alloys, both of which had similar surface morphology as the Nb–Mo alloy. The corrosion products indicated by A in Fig. 5(a) were probably ZrN.

The X-ray diffraction pattern of the Nb–Ru alloy is shown in Fig. 8(b). There were many extra peaks, probably due to the appearance of both ZrN and Nb_2C in it. The peaks of Nb_2C were strong, which means that a large amount of Nb_2C exists on the corroded surface. According to the microstructure shown in Fig. 5(b), there were two types of corrosion products on the surface after the test for 1.08 Ms. Consequently, a large corrosion product indicated by A and a small corrosion

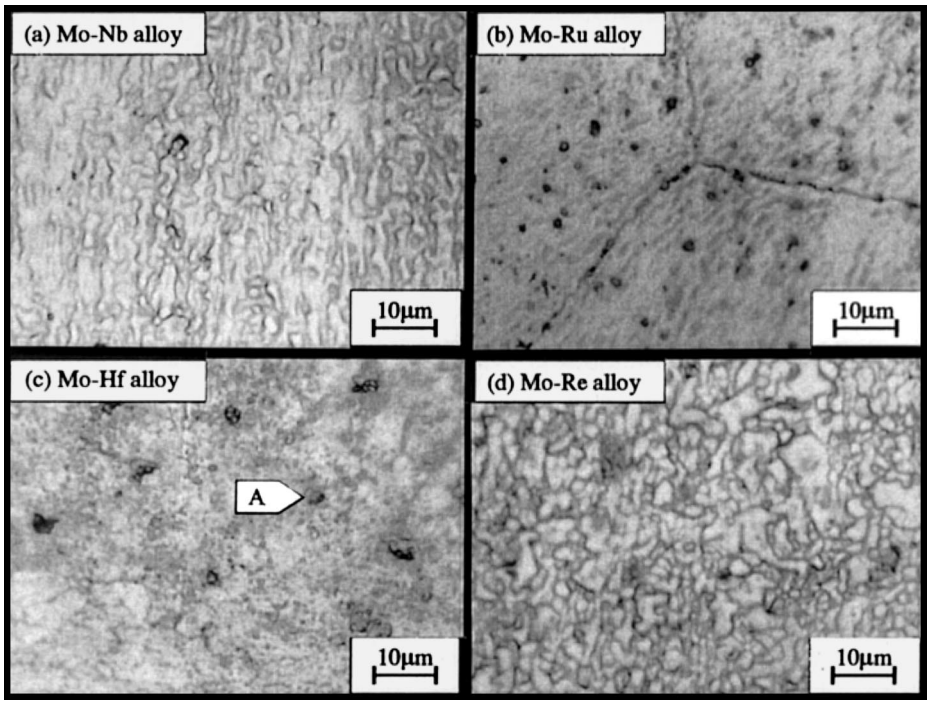

Fig. 7. Surface morphology of Mo-based alloys taken after the corrosion test for 1.08 Ms at 1473 K.

product indicated by B were supposed to be ZrN and Nb_2C, respectively. A similar diffraction pattern was also observed in the Nb–Re alloy, in agreement with the observation of the surface morphology shown in Fig. 5(b). In addition, Nb_2C was not detectable in the Nb–W alloy by the X-ray diffraction, but a small amount of Nb_2C was still present in it, as explained later.

The X-ray diffraction pattern of the Nb–Hf alloy is shown in Fig. 8(c). No extra peaks were found besides the peaks of bcc Nb, in agreement with the microscopic observation in Fig. 5(c).

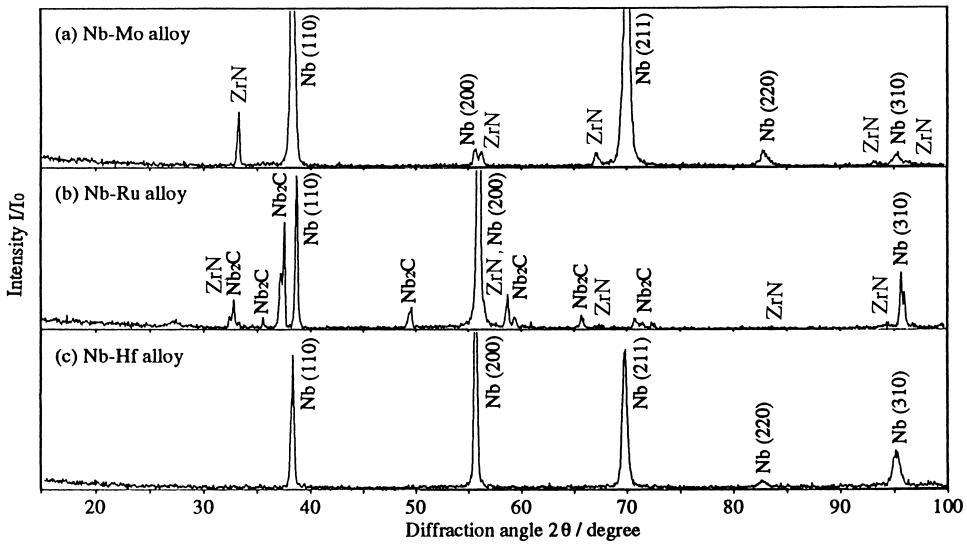

Fig. 8. X-ray diffraction patterns of (a) Nb–Mo, (b) Nb–Ru and (c) Nb–Hf alloys, obtained after corrosion test for 1.08 Ms.

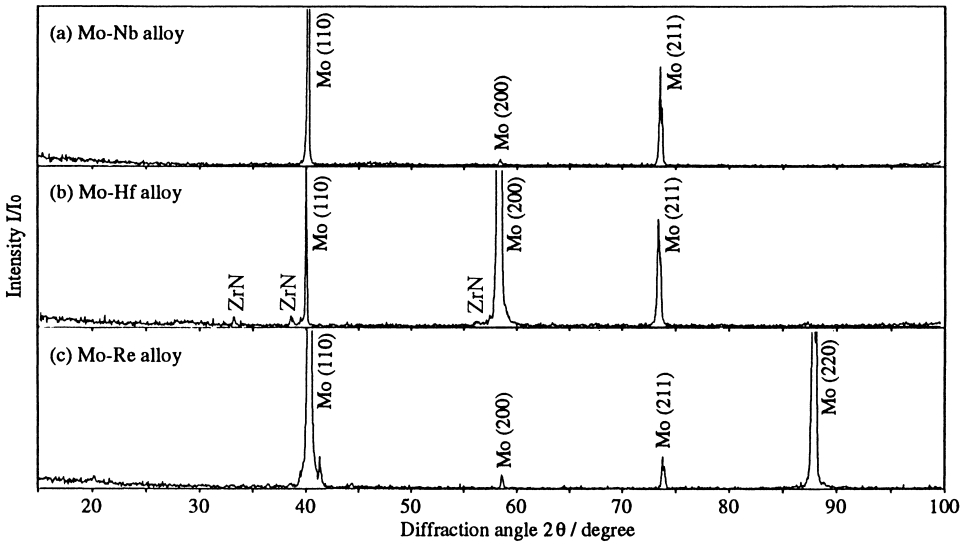

Fig. 9. X-ray diffraction patterns of (a) Mo–Nb, (b) Mo-Hf and (c) Mo-Re alloys, obtained after corrosion test for 1.08 Ms.

3.3.2. Mo-based alloys

The X-ray diffraction pattern is shown in Fig. 9(a) for the Mo–Nb alloy after the corrosion test for 1.08 Ms. There was three strong peaks of bcc Mo, but no extra peaks from the corrosion products were seen in Fig. 6(a), probably due to a limited amount of the corrosion products in it.

There were a few extra peaks in the X-ray diffraction pattern of the Mo–Hf alloy as shown in Fig. 9(b). However, they were much weaker in the intensity compared to the peaks of bcc Mo. These peaks may come from the corrosion product indicated by A in Fig. 7(c). They may be identified with the peaks from ZrN.

The X-ray diffraction pattern of the Mo–Re alloy, which had a similar surface morphology as the Mo–Nb alloy, is shown in Fig. 9(c). Compared to the X-ray pattern of the Mo–Nb alloy shown in Fig. 9(a), there were a few extra peaks which were not able to be identified. The diffraction pattern of the Mo–W alloy was similar to that of the Mo–Re alloy.

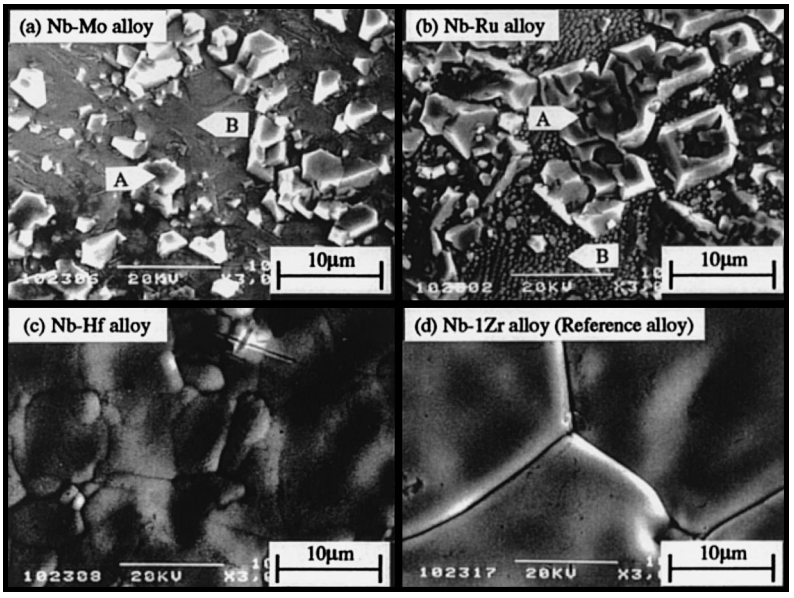

Fig. 10. Surface morphology of Nb-based alloys observed after corrosion test for 1.08 Ms at 1473 K.

3.4. EPMA analysis

3.4.1. Nb-based alloys

There were lots of corrosion products on the corroded surface in the Nb–Mo alloy after the corrosion test for 1.08 Ms as shown in Fig. 10(a). There was a large amount of Zr and also a small amount of Hf in the corrosion product indicated by A in the figure. Similar results were also obtained for the corrosion products in the Nb–Ta and the Nb–W alloys. The matrix region in these alloys contained the alloying element of more than 5.5 at.%. In other words, the concentration of the alloying element was higher on the surface than the average value, 5 at.%, in the bulk. From this result, it was supposed that Nb atoms were dissolved into liquid Li more easily than the alloying element in the Nb–Ta and the Nb–W alloys.

The two types of corrosion products were observed in the Nb–Ru alloy as shown in Fig. 10(b). They were denoted by A and B in the figure. The surface was nearly covered by the two types of the corrosion products. There was a large amount of Zr in the larger corrosion product, A, in this alloy. About 4.4 at.% Ru was detected in the matrix region where corrosion products did not exist. Thus the concentration of the alloying element was slightly lower on the surface than in the bulk, in contrast to the results of Nb–Ta and Nb–W alloys. This means that a small amount of Ru was dissolved into liquid Li.

The uniformly corroded surface is shown in Fig. 10(c) for the Nb–Hf alloy and (d) for the Nb–1Zr alloy. There was no corrosion product on the surface. The sub-grain boundary was observed in the Nb–Hf alloy. Also, the grain boundary of the Nb–1Zr alloy was deeply corroded. About 3.3 at.% Hf was detected on the surface of the Nb–Hf alloy. This means that Hf atoms were dissolved into liquid Li.

3.4.2. Mo-based alloys

The surface morphology after the corrosion test for 1.08 Ms is shown in Fig. 11(a) for Mo–Nb (b) for Mo–Ru and (c) for Mo–Hf alloys. The surface of the Mo–Nb alloy was covered by small granular corrosion products as shown in Fig. 11(a). From the Energy Dispersive X-ray spectroscopy (EDS) analysis, this corrosion product was found to have the composition near a Mo–34 at.% Zr, even though the Mo composition may be overestimated due to the picking-up of the X-ray signal from the base Mo metal, because the size of the corrosion product (~2 μm) was smaller compared to the incident beam size (~3 μm).

The corrosion products on the Mo–Ru alloy were observed along the grain boundaries and inside the grains as well, as shown in Fig. 11(b). The product formed on the grain boundary was MoRu (B2 type structure) according to the EDS analysis. Also, Zr, Mo and Hf were detected from the corrosion products inside the grains. Thus, there was a compositional difference between the corrosion products formed on the grain boundaries and formed inside the grains.

The surface morphology of the Mo–Hf alloy is shown in Fig. 11(c). About 3.0 at.% Hf was detected on the surface. From this result, it may be said that Hf atoms were dissolved into liquid Li. The similar surface morphology was observed in the Mo–Re alloy, however, about 6.8 at.% Re was detected on the surface, indicating the Re atoms were not dissolved into liquid Li.

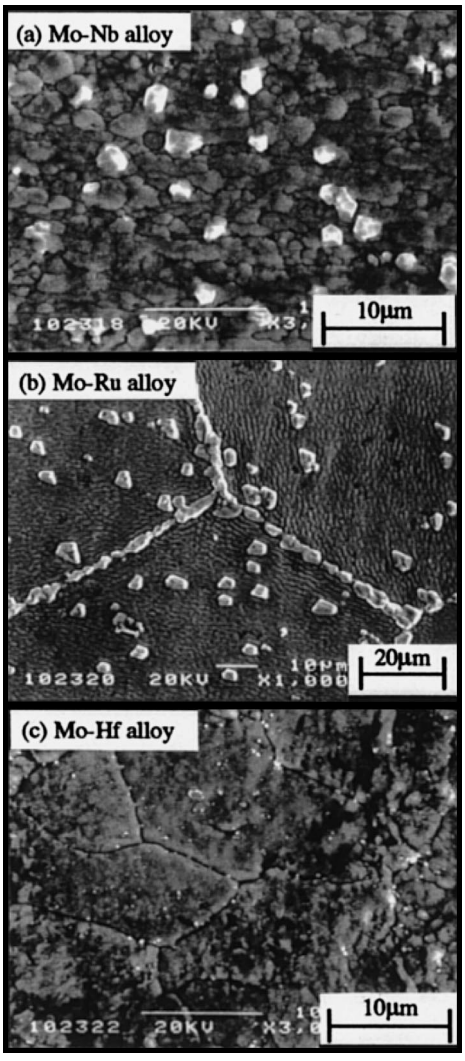

Fig. 11. Surface morphology of Mo-based alloys observed after corrosion test for 1.08 Ms at 1473 K.

4. Discussion

4.1. Nb-based alloys

Corrosion tests of pure metals were carried out previously using the same experimental conditions. Pure Nb showed a large weight gain, about 5.4 g/m^2, after the corrosion test for 1.08 Ms. However, some Nb-based alloys showed the weight loss as shown in Fig. 2. It means that the corrosion behavior changes largely by alloying. In response to this change, surface morphology of binary alloys varied largely depending on the alloying elements, as shown in Fig. 5. Also, as shown in Fig. 2 both the Nb–Ru and the Nb–Re alloys showed a large weight loss, even though there were lots of corrosion products on the surface. Therefore, not only the weight change but also the surface morphology is a good indication to show the corrosion behavior of these alloys.

Two corrosion products were observed in the Nb-based alloys. One is ZrN and the other is Nb_2C, as explained earlier. Both ZrN and Nb_2C are very stable compounds according to the Ellingham diagram for the free energy of formation of nitrides or carbides. The existence of these compounds was further confirmed by measuring the N and C concentration distributions on the corroded surface of Nb–W alloy using Auger electron spectroscopy (AES). On the corroded surface shown in Fig. 12(a) there are lots of large corrosion products indicated by A and small corrosion products indicated by B. From (b) and (c), it was found that nitrogen was present mainly in the large corrosion product, whereas carbon was present in the small corrosion product. Therefore, it was supposed that the large one was ZrN and the small one was Nb_2C.

Session has reported that mass transfer of Zr atoms takes place from high temperature region to low temperature regions [6,7]. Therefore, it is considered that the Zr atoms are firstly dissolved into liquid Li from the capsule and the holder, both of which are made of Nb–1Zr alloy, and then combined with nitrogen atoms, and finally ZrN is deposited on the surface of specimens. Here, nitrogen atoms interacting with Zr atoms may come from liquid Li. This is because the nitrogen content in liquid Li was 5–20 ppm after corrosion test, which was much lower than the original value before the corrosion tests, 30–90 ppm. It was evident that nitrogen atoms in liquid Li were consumed partially for the formation of ZrN. Similarly, carbon atoms are dissolved into liquid Li from the capsule and the holder, both containing 0.003 wt% C, and probably from the test specimens as well. Such dissolution of carbon atoms into liquid Li is expected to occur in the present case. In fact, for stainless steel, it is known that the decarburization takes place in liquid Na [8,9]. It is likely that Nb atoms are combined with these dissolved carbon atoms in liquid Li, leading to the formation of Nb_2C.

Thus, C and N impurities affected the corrosion behavior of the Nb-based alloys. In addition, oxygen atoms in the metal specimen may play an important role on the corrosion behavior in liquid Li [4,9]. For example, ternary oxides ($Nb_xLi_YO_z$) are formed on the grain boundaries or on certain crystallographic planes, and then some cracks may initiate in them by operating the wedging mechanism. In the present experiment, many

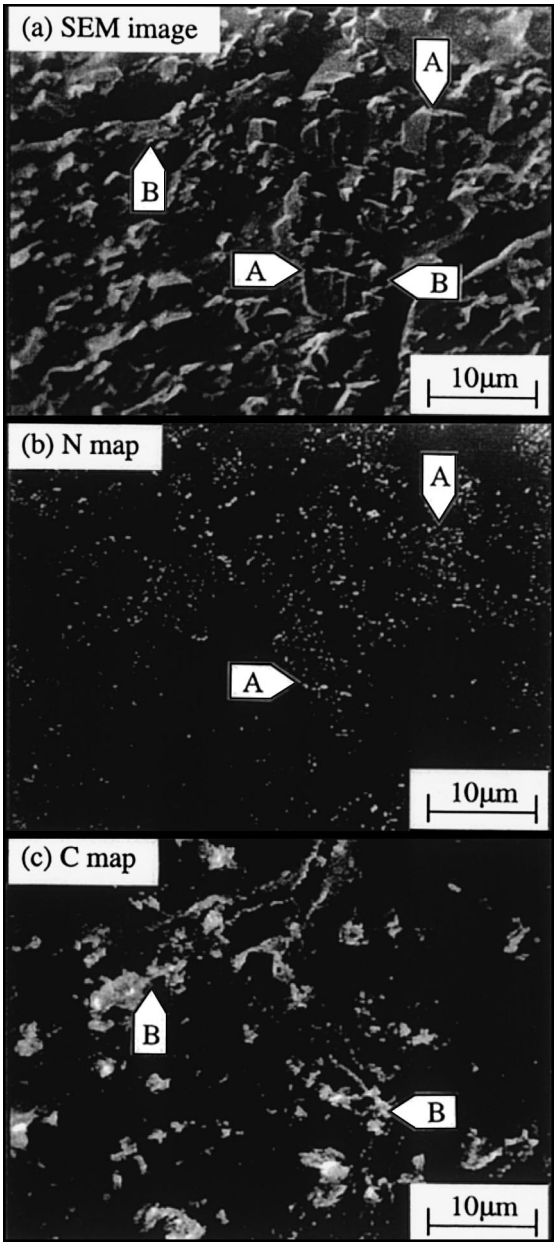

Fig. 12. (a) SEM image, (b) N and (c) C concentration maps on the corroded surface of Nb–W alloy measured using Auger electron spectroscopy.

cracks were also observed on the surface, although the mechanism for cracking is still unknown at the moment.

The weight changes were more moderate for Nb–Mo, Nb–Ta and Nb–W alloys, compared to Nb–Re and Nb–Ru alloys, So, it may be said that the addition of Mo, Ta and W does not affect the corrosion behavior significantly. On the other hand, the weight change was small for the Nb–Hf alloy, and there was nearly no corrosion product on the surface. Also, the corrosion occurred uniformly in this alloy. Therefore, it is evident that Hf is the most effective element in improving corrosion resistance among alloying elements. Zirconium appears to be another effective element, because the corroded surface of the Nb–1Zr alloy was similar to that of Nb–Hf alloy. Both these alloys also exhibited excellent corrosion resistance in liquid Na [5]. Barin has reported that getter elements (e.g., Zr) are effective elements to suppress grain boundary attacking, because those elements can stabilize the dissolved oxygen by forming zirconium oxides [10]. In this experiment, in addition to oxygen, nitrogen and carbon were found to be very important impurities in liquid Li. Zirconium and Hf get the dissolved impurities in liquid Li and stabilize their compounds. Also, Zr and Hf were used for the hot-trap equipment of Li refinement [11]. Such a gettering effect is probably one of the reasons why Nb–Hf and Nb–Zr alloys had good corrosion resistance.

A macro-model for the corrosion of Nb-based alloys in liquid Li was made on the basis of these experimental results, as shown in Fig. 13. The polished surface of a specimen is shown in Fig. 13(a). It is very rough at this initial stage. Then, the corrosion occurs uniformly and the surface becomes smooth as shown in Fig. 13(b). Subsequently, the corrosion products adsorb on the corroded surface as shown in Fig. 13(c). Finally, they grow up and their number increases. At this stage, cracks initiate on the corroded surface. But the mechanism for the cracking still remains unknown.

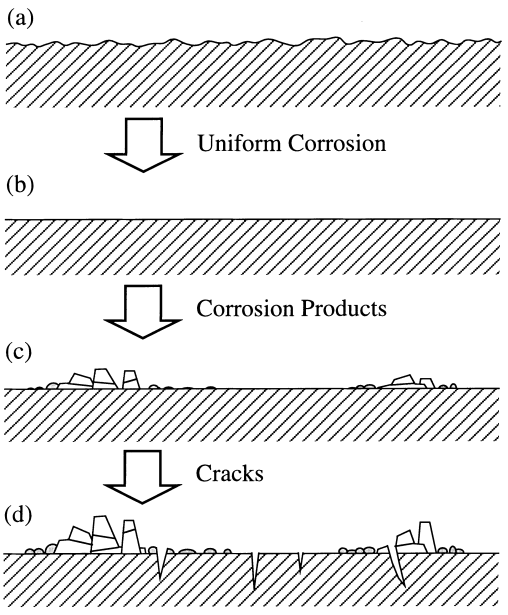

Fig. 13. Schematic drawing of corrosion sequence of Nb-based alloys in liquid Li.

4.2. Mo-based alloys.

Pure Mo showed a large weight loss, about 1.8 g/m^2, after the corrosion test for 1.08 Ms. The weight loss turned to the weight gain by the addition of alloying elements except for Ru, and the amount of the weight change was smaller in the Mo-based alloys than in pure Mo. Thus, the addition of alloying elements to pure Mo could improve the corrosion resistance in liquid Li. Furthermore, it is supposed that those alloys which contain alloying elements with a stronger affinity for impurity elements such as C, N and O, exhibit higher corrosion resistance. For example, Hf is such an alloying element, and the Hf addition is very beneficial to the further enhancement of the corrosion resistance.

The weight change was about 10 times smaller for the Mo-based alloys than for the Nb-based alloys. Roy suggested that Mo-based alloys can be used at the temperatures higher than 1623 K [12]. In contrast, Nb-based alloys are corrosive around 1523 K or at the flow velocity of about 6 m/s in liquid Li. DiStefano et al. reported that the Nb–1Zr alloy coated with a thin Mo film showed high corrosion resistance at 1073 K [4]. Also, even in case of liquid Na, the weight loss of the Mo-based alloys was about 10 times smaller that of the Nb-based alloys [5]. Therefore, it is apparent that Mo-based alloys have excellent corrosion resistance to liquid metals. The difference of solubilities between Nb and Mo in liquid Li may be related partially to the difference in the corrosion resistance between them. Namely, the solubility of Mo is about 3×10^{-4} wt% at 1473 K, which is much smaller than the solubility of Nb, (about 2.5×10^{-3} wt% at 1473 K) [13,14]. Thus, the less soluble elements exhibit the higher corrosion resistance.

5. Conclusion

The corrosion tests of Nb-based and Mo-based binary alloys were performed for 1.08 Ms in liquid Li at 1473 K. The corrosion resistance was modified strongly by alloying. For example, the addition of Re and Ru reduced remarkably the corrosion resistance against liquid Li. On the contrary, the Nb–Hf alloys showed a very small weight change, and there was no corrosion product on the surface. Hafnium was indeed a beneficial element in improving the corrosion resistance. However, the were many cracks running through the surface of all

the Nb-based alloys at 1473 K. A model for the corrosion sequence was proposed for Nb-based alloys on the basis of the present experimental results.

The binary Mo-based alloys exhibited much higher corrosion resistance than the binary Nb-based alloys. In order to enhance the corrosion resistance further, Hf is probably one of the best alloying elements in these alloys.

References

[1] J.A. Horak, R.W. Swindeman, H.E. McCoy, Oak Ridge National Laboratory Report ORNL/TM-9740, ORNL, 1990.
[2] L.J.Pionke, J.W.Davis, COO–4247-2, McDonnell Douglas Corporation, 1979.
[3] J.R. DiStefano, Oak Ridge National Laboratory Report ORNL-3551, 1966.
[4] J.R. DiStefano, J.W. Hendricks, Nucl. Tech. 110 (1995) 145.
[5] S. Inoue, S. Kano, J. Saito, Y. Isshiki, E. Yoshida, M. Morinaga, in: H.U.Borgstedt (Ed.), Proceedings of the Second International Seminar on Liquid Metal Systems, Karlsruhe, Plenum, New York, 1995, p. 75.
[6] C.E. Session, J.H. De Van, Nucl. Appl. Tech. 9 (1970) 250.
[7] C.E. Session, J.H. De Van, Oak Ridge National Laboratory Report ORNL–TM-1455, 1966.
[8] H. Miura, T. Ito, E. Yoshida, S. Kano, I. Nihei, in: Y. Fruchard (Ed.), Proceedings of the International Conference on Liquid Metal Engineering and Technology, SFEN, Avigon, 1988, p. 505.
[9] C. Adhelhelm, E. Nold, D.Kempf, Liq. Met. Eng. Technol. (1984) 171.
[10] I. Barin, Thermochemical Data of Pure Substance, VCH, Weinheim, Germany.
[11] T. Suzuki, H. Katsuta, J. Atomic Energy Soc. Jpn. 27 (1985) 411.
[12] P. Roy, in: Tsukuba (Ed.), Proceedings of the International Symposium on the Material Chemistry in Nuclear Environment, Technical Program Committee, STA, Tokyo, 1992, p. 181.
[13] R.L. Eichhelberger, R.L. Mckisson, B.G. Johnson, National Aeronautics and Space Administration comtriction Report, CR-1371, 1969.
[14] V.A. Maroni, E.J. Carirns, F.A. Cafasso, Argonne National Laboratory Report ANL-8001, 1973.